geoconvention
Calgary • Canada • May 12-14 2025

Revisiting legacy crooked seismic profiles with 3D multifocusing for enhanced subsurface imaging and structural characterization

Hossein Jodeiri Akbari Fam[1], Ernst Schetselaar[1], Gilles Bellefleur[1], Don White[1], Eric de Kemp[1], and Azadeh Ashoori[1]*

[1]Natural Resources Canada, Geological Survey of Canada

Summary

Deep seismic imaging is crucial for lithospheric studies and resource exploration, provides a comprehensive understanding of deep tectonic zones and enhances 3D subsurface models. A processing scheme based on multifocusing was developed to improve the resolution of seismic images and extract the 3D geometry of subsurface structures from crooked seismic profiles. The structural properties, including curvature, strike, and dip angles, are optimally estimated by maximizing the coherence function, which is defined based on the 3D multiparameter multifocusing operator. Compared to conventional methods, the new stacking operator can estimate traveltimes of reflections and diffractions more accurately by accounting for crooked survey geometry, velocity heterogeneity, topography, and azimuth-dependent dip effects. To effectively estimate the globally optimal properties, a multidimensional constrained differential evolution optimization algorithm was incorporated. However, this process is computationally demanding and requires considerable processing resources. Thereby, we developed a high-performance program using the Cuda-OpenMP paradigm, accelerated and parallelized on a cluster with a hybrid architecture compromised of multiple graphical and central processing units. The new workflow was applied to the reprocessed regional-scale LITHOPROBE seismic profile (~410 km, E-W) along the Trans-Hudson Orogen transect. Our approach significantly improved the quality of the seismic image and provided valuable structural constraints, which enhanced subsurface structural interpretation and allowed for a more detailed delineation of subsurface structures in three dimensions.

Introduction

While a full 3D seismic survey is typically necessary to capture the 3D structure of subsurface features, crooked-line seismic surveys can also effectively provide this information (Malehmir and Bellefleur, 2016). Despite the technical challenges in processing crooked-line seismic surveys, they improve data coverage by capturing a wider range of ray paths with distinct azimuths, which enable capturing 3D geometry of the subsurface (Wu, 1996; Schmelzbach et al., 2007; Jodeiri Akbari Fam et al., 2021; 2022; 2023a).

The Flin Flon Domain (FFD) in northern Manitoba and Saskatchewan offers a wealth of information from years of study, providing a natural geophysical and geological laboratory for testing new methods. We selected a 410 km long 2D crooked regional seismic line, which was acquired in 1991 as part of the LITHOPROBE initiative (Lewry et al., 1994; White et al., 2005) along the Trans-Hudson Orogen (THO) transect, extending from the Flin Flon belt in the east to the Hearne craton in the west (Lucas et al. 1993).

The western FFD, located within the Reindeer Zone (RZ) of the Paleoproterozoic THO formed mostly between ca. 1.92-1.88 Ga (Lucas et al., 1996). The belt consists of juvenile arc and back-arc assemblages, comprising volcanic, plutonic, and sedimentary rocks that were accreted and deformed during the collision between the Superior, Sask and Hearne cratons (Ashton et al., 2005; Corrigan et al., 2005). These volcanic assemblages host significant volcanogenic massive sulfide (VMS) deposits, formed during periods of volcanic quiescence within the arc system (Syme and Bailes, 1993; Gibson et al., 2007). Recent research highlights the role of hydrothermal activity associated with extensional tectonics during these quiescent periods in focusing sulfide mineralization (Galley et al., 2007).

The structural evolution of the FFD records a complex history of accretionary tectonics and subsequent deformation. The belt underwent early thrust-related deformation, followed by multiple episodes of folding and strike-slip faulting (Ashton et al., 2005; Corrigan et al., 2005, Hammer et al., 2009; Lafrance et al., 2016). Transpressional tectonics likely played a key role in these deformational phases, as indicated by regional structural trends and kinematic analyses (Ansdell, 2005). Metamorphic conditions vary across the belt, with areas of lower metamorphic grade preserving primary volcanic and sedimentary structures (DeWolfe et al., 2009). The tectonic framework reflects the progression from arc construction through accretion to final modification during craton collision (Lucas et al., 1996).

First, we review the theory of the 3D multifocusing seismic imaging method. Then, we describe the conventional processing and multifocusing workflows applied to the seismic profile and present the resulting images and structural constraints. Next, we compare the conventional and multifocusing results. Lastly, we discuss how the proposed method can enhance structural interpretation and regional-scale 3D modelling and explore the implications of the multifocusing method for exploration.

Method

Jodeiri Akbari Fam et al. (2023b) proposed the 3D generalized spherical multifocusing (GSMF) algorithm to generate a high-resolution seismic section or image volume from crooked-line or 3D seismic field data acquired in regions with heterogeneous overburden and complex subsurface. This approach accounts for the elevation and spatial coordinates of both source and receiver positions which enables its application to seismic data acquired with an arbitrary recording configuration over an area with irregular topography. The method simultaneously corrects for nonhyperbolic moveout and azimuth-dependent dip-moveout effects. Unlike depth imaging techniques, this algorithm is data-driven and does not require prior knowledge of the subsurface model (Landa et al., 2009). Instead, it requires estimating four unknown 3D wavefield parameters simultaneously using a nonlinear global optimization method, such as the differential evolution (Storn and Price, 1997; Jodeiri Akbari Fam et al., 2023a; 2023c) or the very fast simulated annealing algorithms based on coherence analysis (Jodeiri Akbari Fam and Naghizadeh, 2019). These parameters can eventually be transformed into structural information, including strike, dip, and curvature.

Figure 1a illustrates the reflection ray geometry (the dashed blue line) for an arbitrary seismic survey setup over a reflector with an uneven interface embedded in a constant-velocity (v_0) medium with irregular topography. The 3D GSMF method aims to accurately compute the

traveltime of the seismic reflection and estimate the spatial coordinates of the reflection point, ultimately providing detailed insights into subsurface structures. The core concept involves fitting a series of spheres with varying curvatures and centers to locally model the geometry of the reflector. The curvature and center of each sphere are iteratively adjusted to replicate the reflection traveltime response observed in the seismic trace recorded at the surface. In fact, this iterative process decomposes the prestack seismic wavefield from a complex interface into responses from a series of spherical surfaces, each associated with a specific curvature and origin at every imaging point ($[x_I, y_I, z_I]$) and time step (t_0). A more detailed formulation is provided in the original article by Jodeiri Akbari Fam et al. (2023b) that describes the reflection traveltime

$$t(x_I, y_I, z_I, t_0) = f(v_0, \beta, \varphi, R_N, R_{NIP}) \tag{1}$$

as a function of curvature and origin of spheres, which can be linked to wavefield attributes, as shown in Figure 1b. The wavefield attributes include the emergence (β) and azimuthal (φ) angles of the zero-offset normal ray originating from the imaging point (I) and the radii of curvature for both the normal (R_N) and normal-incidence-point waves (R_{NIP}). The wavefield attributes describe distinct physical properties of the reflector (Xie and Gajewski, 2018). Thus, their optimal estimation through coherence analysis allows the approximation of subsurface structural properties, such as dip, dip direction, and curvature. Furthermore, this method provides coherence, a measure of estimation certainty.

$$\begin{cases} Dip\ (x_I, y_I, z_I, t_0) \\ Dip\ direction\ (x_I, y_I, z_I, t_0) \\ Curvature\ (x_I, y_I, z_I, t_0) \\ Coherence\ (x_I, y_I, z_I, t_0) \end{cases} \tag{2}$$

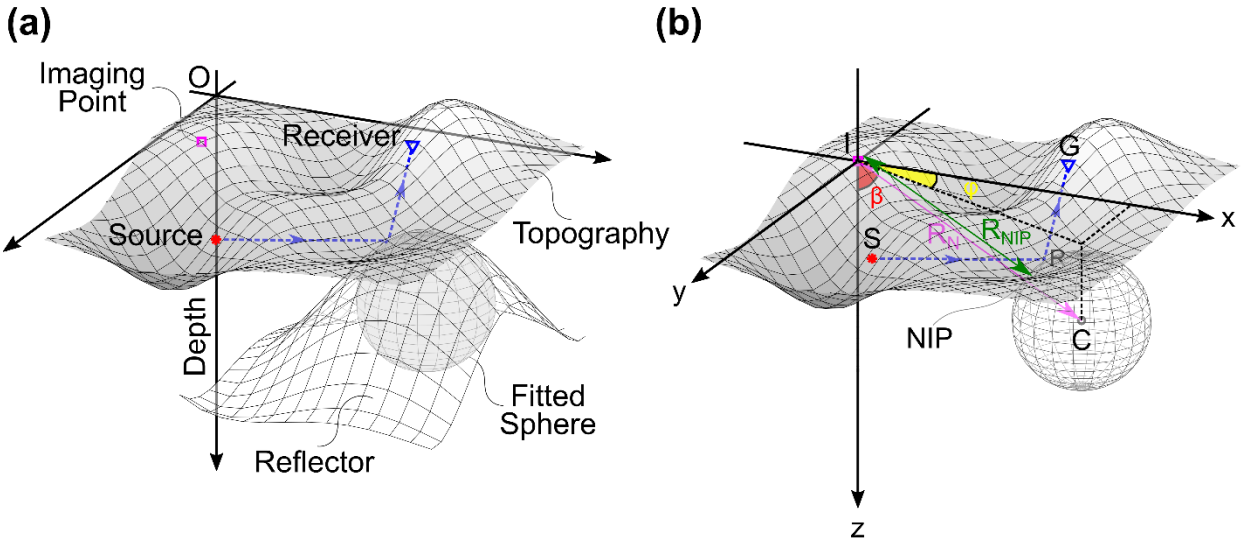

Figure 1: Schematic diagram of the 3D generalized spherical multifocusing method (adapted from Jodeiri Akbari Fam et al., 2023b).

Results

We examined our data-driven seismic processing workflow to improve the quality of the subsurface image and extract structural information, which results in more accurate delineating of subsurface structures. Figure 2 presents a perspective view of the bedrock geological map on the surface and the seismic images of the crooked seismic LITHOPROBE line 9. These images were produced using two distinct seismic processing workflows, including Kirchhoff time migration of the conventional stack (Figure 2a) and phase shift plus interpolation (PSPI) time migration of the multifocusing stack (Figure 2b). The results demonstrate the improvements achieved by the 3D GSMF approach over the conventional processing method.

Table 1 outlines the summary of processing sequences applied in both conventional and multifocusing workflows. The conventional processing sequence was conducted by Western Atlas International-Western Geophysical in 1992. As outlined in Table 1, they followed a standard processing flow, which included poststack time migration of the normal moveout-corrected stack section. To apply the multifocusing technique, we reprocessed the raw field records. After setting the survey geometry up and picking the first arrivals, a 2D velocity-depth model of the near-surface was constructed using a non-linear traveltime tomography method to correct elevation and weathering statics. A sequence of signal processing steps was applied to reduce both coherent and random noise while partially restoring the reflection and diffraction amplitudes (Yilmaz, 2001). Crooked-line binning was applied, and the processed field records were sorted into super common-cell gathers, each consisting of five adjacent cells. Super binning increased the fold by a factor of five and provided appropriate offset distribution and distinct azimuths to capture the geometry of the subsurface structure in 3D.

Next, wavefield attribute analysis was conducted to optimally estimate the unknown parameters by maximizing the coherence function (Jodeiri Akbari Fam et al., 2023a). Figure 2c displays the coherence values for each estimation across all time steps and image locations, indicating the confidence level in coherently stacking reflections and optimally estimating wavefield parameters. Multifocusing stacking was then applied to the super common cell gathers. This step corrects azimuth-dependent normal and dip moveout and resolves the non-hyperbolicity of reflections and diffractions. Imaging of the subsurface was achieved through PSPI time migration using a constant velocity of 6000 m/s. In the final stage, postmigration filtering was used for better visualization, and the processed time-domain data were converted to depth for geological interpretation and integration with field measurements. The migrated multifocusing stack image (Figure 2b) highlights enhanced resolution and improved continuity of subsurface reflectors compared to the migrated conventional stack (Figure 2a). Additionally, this comparison reveals that not only the new workflow focused reflectors with better continuity but also identified new ones.

Table 1. Summary of processing sequences applied to LITHOPROBE (Line 9) profile in the conventional and multifocusing workflows.

Conventional	Multifocusing
– Setting up the geometry – Picking the first breaks	
– Field Statics – Amplitude recovering – Deconvolution – Statics corrections – Residual statics – Muting the first arrivals – Crooked-line binning – Velocity analysis – NMO correction – Trim Statics – Stacking – Random noise attenuation – F-K Stolt migration (constant velocity of 6000 m/s)	– 2D near-surface velocity-depth modelling – Source-receiver statics corrections – Residual statics corrections – Amplitude recovering – Spiking deconvolution – Muting the first arrivals – Crooked-line binning – Super common cell gathering – Wavefield attributes analysis – 3D GSMF moveout correction – Stacking – PSPI time migration (constant velocity of 6000 m/s)
– Postmigration filtering – Time-to-depth conversion	

In addition, we derived dip and dip-direction angles from the optimal wavefield parameters and migrated them to their correct special locations. Figure 3 shows a perspective view of the bedrock geological map on the surface and the structural properties derived along the profile. Figure 3a is the true dip angle section ranging from 0 to 60 degrees and Figure 3b is the true dip-direction section ranging from 0 to 360 degrees, where 0 is pointing to the north. Figure 3c depicts representative structural properties (dip and dip direction) using tablets, co-rendered with the gray-scaled multifocusing seismic image from Figure 2b, to better understand the 3D perspective of high-coherent reflectors. Figure 4 shows structural properties derived using the proposed method within a defined depth window of 1 km along the selected reflectors indicated in Figure 3c for reference. In each Wulff stereonet with equal angle projection, black points represent the poles, the red circle marks the average of the most representative poles, and the red curve traces the plane associated with the average pole. The contours depict the density map of the poles, providing a visual representation of their distribution in the polar coordinate system.

The dashed black rectangles in Figure 2 highlight the cropped areas shown in Figure 5. These cropped sections show that the conventional method (the first column) exhibits limited detail and less quality, while the multifocusing approach (the second column) achieves superior image quality. Structural information derived through applying the multifocusing approach shown with tablets, co-rendered with wiggle traces from the multifocusing image (the last column), provides 3D views of the extracted structural information (e.g., dip and dip-direction constraints). In the last column, the insets present magnified structural details from a distinct perspective which improves spatial insight. Each row corresponds to a different window, labelled for reference.

The first column in Figure 5a shows an abrupt termination of reflectors at mid-crustal depths of the conventionally processed section. This termination was interpreted as the steeply east-dipping subsurface trace of the Sturgeon Weir shear zone, offsetting the top of the Sask Craton for about 10 km (Lewry et al., 1994; White et al., 2005). The crookedness of the survey line, however, dispersed midpoints off the survey line, which the conventional 2D imaging method could not accurately resolve. Accounting for the midpoint dispersion along this segment and correcting the cross-dip effect, our method reconstructed coherent and continuous reflectors with a high S/N across the surface trace of the SWSZ (the second column in Figure 5a) disproving the large vertical offset of the historic interpretation.

Additionally, about 25 km farther east, following the band of linear reflectors at the far east end on top 20 km of the profile (Figure 2b) upward to their surface projections and tying with adjacent high-resolution Denare Beach seismic profile (Jodeiri Akbari Fam et al., 2025; Schetselaar et al., 2022a; 2022b) reveals those reflectors are associated with SWSZ. Pandit et al. (1998) also reported that the extreme crookedness of the survey line caused significant distortion in the apparent dip of seismic events, with values ranging from nearly zero to opposite the dip of neighbouring traces, sometimes extending down to 3–4 s. They reprocessed the eastern segment of line 9 by applying a variable cross-dip correction to the normal-moveout-corrected gathers to improve the correlation between the surface geology and the seismic subsurface image. Their approach resolved the discrepancy between a steeply dipping SWSZ and the shallowly east-dipping mylonite foliation recorded at its surface trace (Pandit et al., 1998).

Farther west, the enhanced profile displays true sub-seismic offsets associated with the subvertical Tabbernor fault (TF) zone. This segment displays relatively steep reflectors on opposite sides of the offset, characterized by highly variable strike-dip orientations (Figure 5b), which is consistent with the post-collisional, predominant brittle deformation history of this structure (Ashton et al., 2005 and references therein). The reflectors indicate an apparent vertical displacement of approximately 3.5 km, with the eastern segment upthrown and the western segment downthrown. Seismic reflectors at depths greater than 5 km, however, appear to be continuous across its trace, which either suggests that the TF has an upper crustal depth extent or flattens and diffuses into a fault zone with a shallower dip. A more in-depth interpretation is necessary to support the preliminary findings and address any outstanding questions.

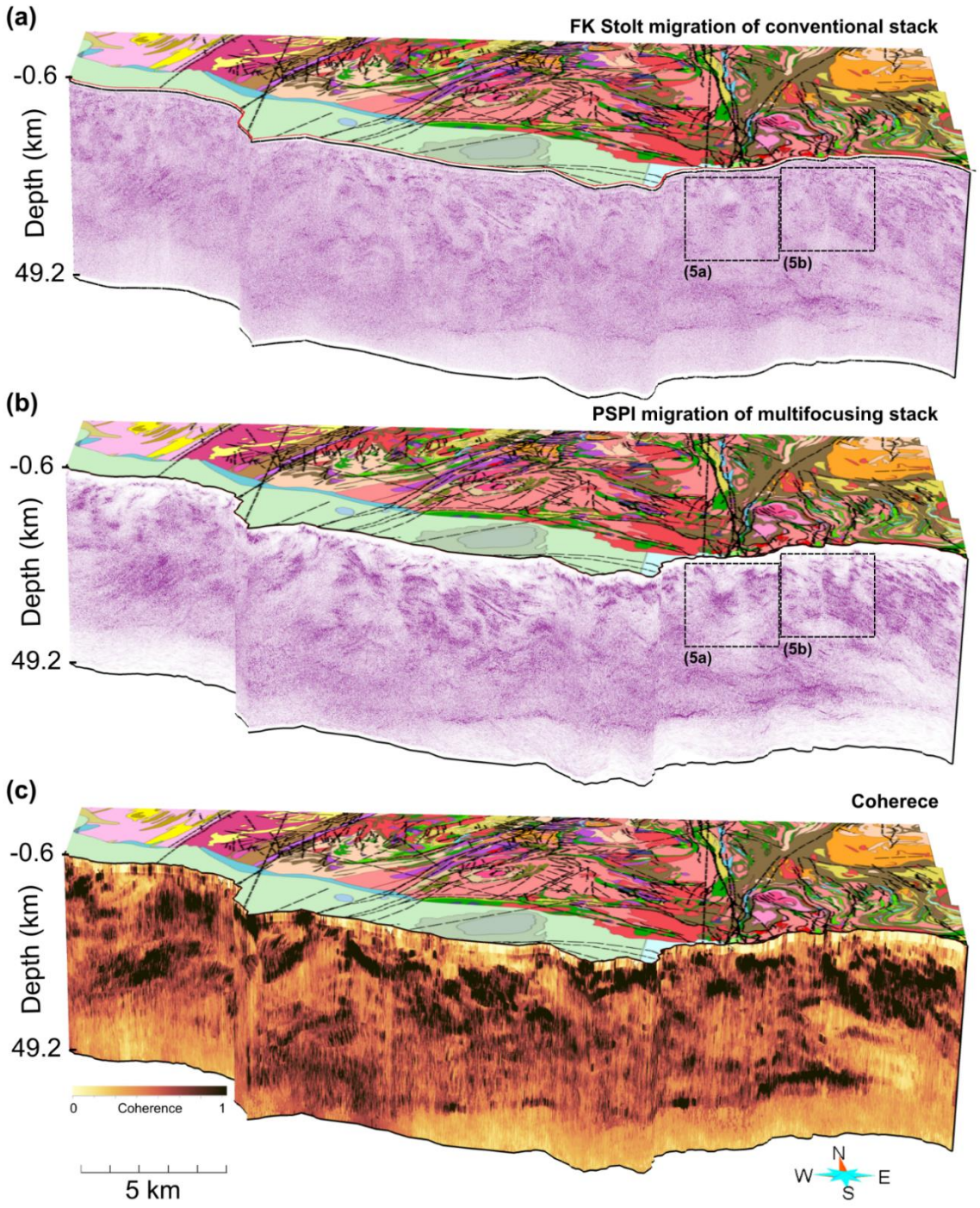

Figure 2: Perspective view of the bedrock geological map and the regional-scale seismic image of crooked LITHOPROBE transect. (a) FK Stolt migration of the conventional stack, (b) PSPI migration of the multifocusing stack, and (c) the coherence section. The dashed black rectangles indicate cropped images shown in Figure 5.

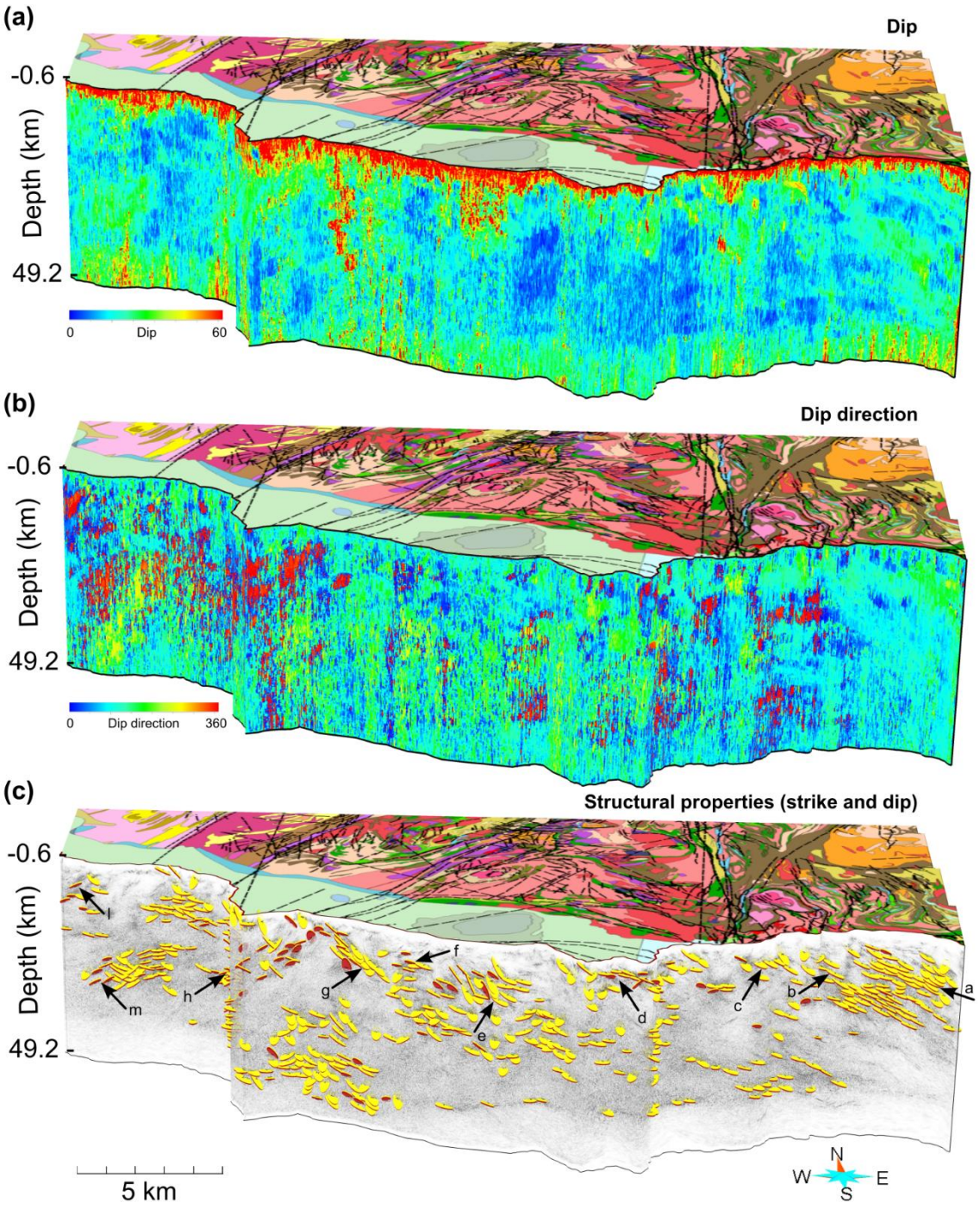

Figure 3: Perspective view of the bedrock geological map and the structural properties. (a) Dip, (b) dip direction, and (c) structural tablets co-rendered with the grayscale image from Figure 2b. The arrows indicate the selected reflectors, whose associated structural properties are displayed using the stereonet in Figure 4.

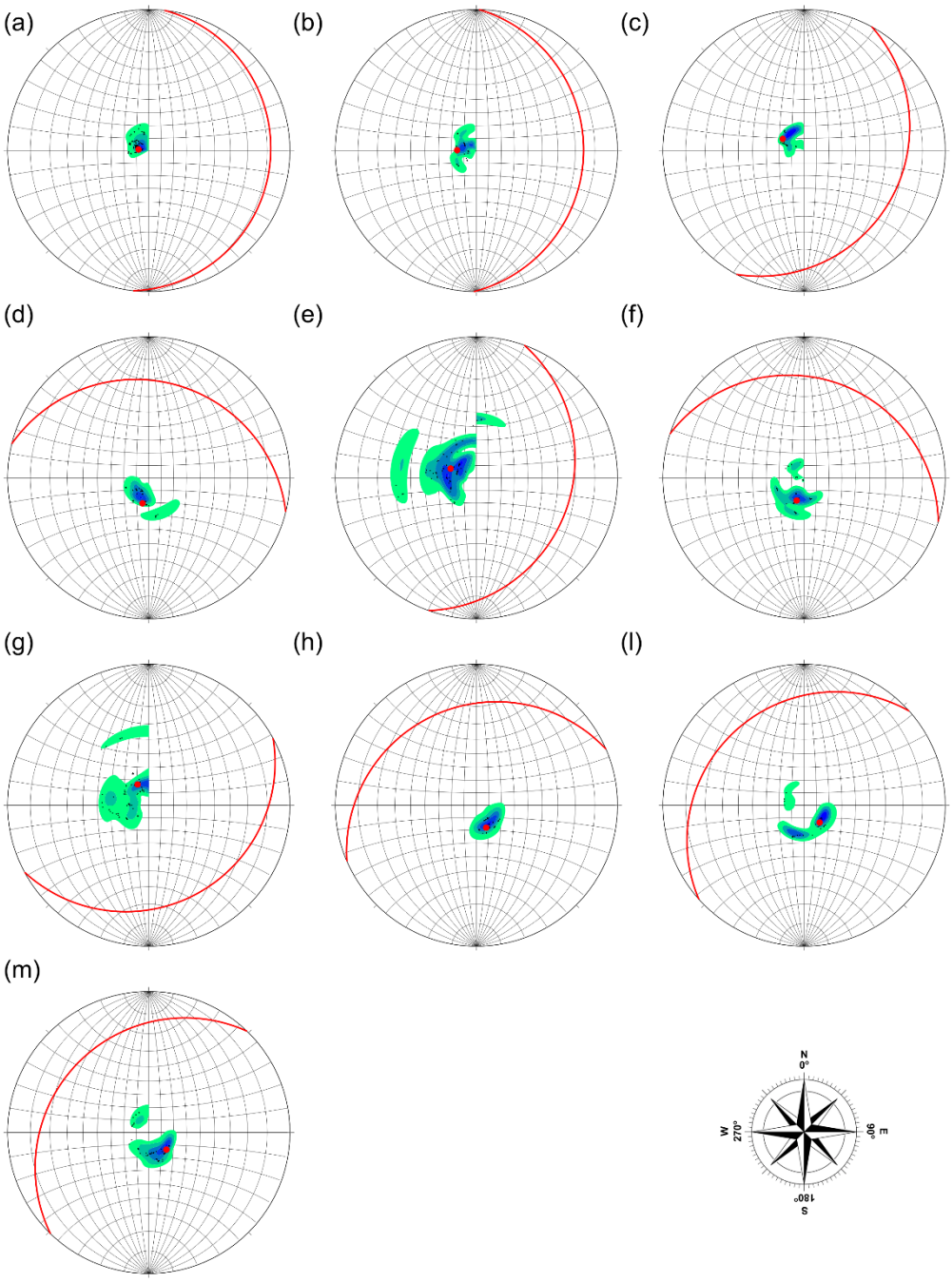

Figure 4: Structural properties derived using the multifocusing method along the selected reflectors labelled in Figure 3c. They are displayed in the Wulff stereonet with equal angle projection, black points represent the poles, the red circle marks the average of the most representative poles, and the red curve traces the plane associated with the average pole. The contours depict the density map of the poles.

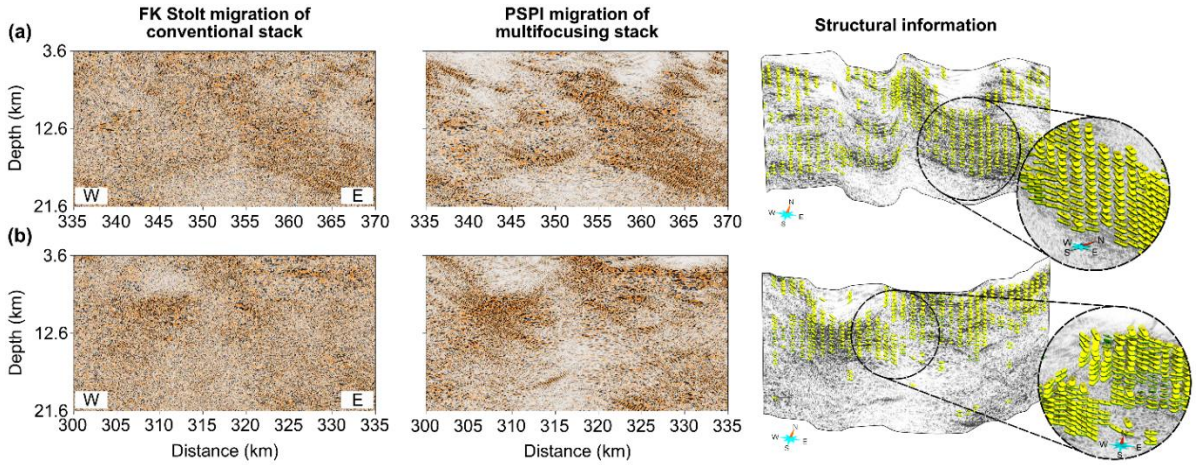

Figure 5: Comparison of the cropped images from LITHOPROBE Line 9. The columns, from left to right, display (1) FK Stolt migration of the conventional stack, (2) PSPI migration of the multifocusing stack, and (3) structural information shown using tablets co-rendered with wiggle traces from the multifocusing image displayed in the second column. The seismic images in (a) and (b) correspond to the windows shown in Figure 2. The seismic interpretation of these windows is discussed in the text.

Conclusions

This study deepened our understanding of the complex subsurface structures and provided insights into the crustal geological framework in the Flin Flon Domain. The multifocusing method significantly enhanced the image quality and signal-to-noise ratio of the regional scale deep seismic profile. Our workflow was able to image more coherent and continuous reflectors compared to the conventional workflow. Additionally, the proposed method provided structural information, which eventually improves subsurface structural interpretation and enables a more refined delineation of subsurface structures in three dimensions. As a result, applying the introduced approach resolved ambiguities in subsurface architecture, which can reduce uncertainty in 3D geological models and ultimately provide reliable models for effective resource prospecting.

Additive Information

Although this study was conducted at a crustal scale, it has opened the possibility of applying it on a more local scale. During the early stages of exploration in a mining camp, when it is not feasible to acquire complete 3D seismic data, this method can extract 3D information from strategically placed 2D profiles or sparse 3D seismic surveys. This technique can effectively image complex geological structures such as vein systems, irregular ore bodies, and stratigraphic traps with greater clarity. Additionally, this method enables the imaging of small-scale features that are often poorly resolved in conventional seismic imaging, including fracture networks caused by faults and shear zones.

Acknowledgements

This research is funded by the Targeted Geoscience Initiative (TGI) and the Critical Minerals Geoscience and Data (CMGD) program. This study is a collaboration between the Federal, Manitoba and Saskatchewan geological surveys, and industry, aiming to improve the effectiveness of deep mineral exploration. The proposed method was executed on Amazon Web Services (AWS).

References

Ansdell, K.M., 2005. Tectonic evolution of the Manitoba-Saskatchewan segment of the Paleoproterozoic Trans-Hudson orogen, Canada; Canadian Journal of Earth Sciences, v. 42, no. 4, p. 741-759.

Ashton, K.E., Lewry, J.F., Heaman, J.M., Hartlaub, R.P., Stauffer, M.R., and Tran, H.T., 2005. The Pelican Thrust Zone: basal detachment between the Archean Sask Craton and Paleoproterozoic Flin Flon – Glennie Complex, western Trans-Hudson Orogen; Canadian Journal of Earth Sciences v. 42, no. 4, p. 685-706, https://doi.org/10.1139/e04-035

Corrigan, D., Hajnal, Z., Németh, B. and Lucas, S.B., 2005. Tectonic framework of a Paleoproterozoic arc-continent to continent-continent collisional zone, Trans-Hudson Orogen, from geological and seismic reflection studies; Canadian Journal of Earth Sciences, v. 42, no. 4, p. 421-434.

DeWolfe, Y.M., Gibson, H.L. and Piercey, S.J., 2009. Petrogenesis of the 1.9 Ga mafic hanging wall sequence to the Flin Flon, Callinan, and Triple 7 massive sulphide deposits, Flin Flon, Manitoba, Canada; Canadian Journal of Earth Sciences, v. 46, no. 7, p. 509-527.

Galley, A.G., Hannington, M. D. and Jonasson, I.R., 2007. Volcanogenic massive sulphide deposits. In: Mineral Deposits of Canada: A Synthesis of Major Deposit Types. Geological Survey of Canada, Mineral Deposits Division Special Publication (5). Geological Association of Canada, St. John's, Newfoundland and Labrador, p. 141-162.

Gibson, H.L., Allen, R.L., Riverin, G. and Lane, T.E., 2007. The VMS model: Advances and application to exploration targeting; In Proceedings of Exploration, v. 7, p. 713-730.

Hammer, P.T.C., Clowes, R.M. Cook, F.A., van der Velden, A.J., Vasduvan, K. 2009. The Lithoprobe trans-continental lithospheric cross sections: imaging the internal structure of the North American continent, Canadian Journal of Earth Sciences, v. 47, p. 821–857, https://doi.org/10.1139/E10-036

Jodeiri Akbari Fam, H. and Naghizadeh, M., 2019. Multi-focusing stacking using the very fast simulated annealing global optimization algorithm; GeoConvention, Extended Abstracts.

Jodeiri Akbari Fam, H., 2022. Multifocusing seismic imaging of complex geological structures; Ph.D. thesis, Laurentian University, Canada, https://laurentian.scholaris.ca/handle/10219/4004

Jodeiri Akbari Fam, H., Naghizadeh, M., and Yilmaz, Ö., 2021. 2.5D multifocusing imaging of crooked-line seismic surveys; Geophysics, v. 86, no. 6, p. S355–S369, https://doi.org/10.1190/geo2020-0660.1

Jodeiri Akbari Fam, H., Naghizadeh, M., Smith, R., Yilmaz, Ö., Cheraghi, S., and Rubingh, K., 2023a. High-resolution 2.5D multifocusing imaging of crooked seismic profile in a crystalline rock environment: results from the Larder Lake area, Ontario, Canada; Geophysical prospecting, Special Issue: Mineral Exploration and Mining Geophysics, v. 71, no. 7, p. 1152–1180.

Jodeiri Akbari Fam, H., Naghizadeh, M., Yilmaz, Ö., and Smith, R., 2023b. 3D generalized spherical multifocusing seismic imaging; Geophysics, v. 88, no. 1, p. T13–T31, https://doi.org/10.1190/geo2022-0154.1

Jodeiri Akbari Fam, H., Naghizadeh, M., Yilmaz, Ö., Smith, R., and Esmaeilzadeh, N., 2023c. 3D spherical multifocusing stack over an irregular topography: A data-driven approach for high-resolution seismic imaging in complex geological settings; International Meeting for Applied Geoscience & Energy.

Jodeiri Akbari Fam, H., Schetselaar, E., Bellefleur, G., White, D., de Kemp, E., and A. Ashoori, 2025, Enhanced subsurface imaging with the 3D multifocusing algorithm: 3D geological insights from crooked seismic profiles of the Flin Flon Domain, Reindeer Zone, Saskatchewan – Manitoba; Geological Survey of Canada, TGI Synthesis Volume.

Landa, E., Keydar, S. and Moser, T.J., 2009. Multifocusing revisited-inhomogeneous media and curved interfaces; Geophysical Prospecting, v. 58, no. 6, p. 925–938, https://doi.org/10.1111/j.1365-2478.2010.00865.x

Lewry, J.F., Hajnal, Z., Green, A., Lucas, S.B., White, D., Stauffer, M.R., Ashton, K.E., Weber, W. and Clowes, R., 1994. Structure of a Paleoproterozoic continent-continent collision zone: a LITHOPROBE seismic reflection profile across the Trans-Hudson Orogen, Canada; Tectonophysics, v. 232, no. 1-4, p. 143-160.

Lucas, S.B., Green, A., Hajnal, Z., White, D., Lewry, J., Ashton, K., Weber, W. and Clowes, R., 1993. Deep seismic profile across a Proterozoic collision zone: surprises at depth; Nature, v. 363, p. 339–342, https://doi.org/10.1038/363339a0

Lucas, S.B., Stern, R.A., Syme, E.C., Reilly, B.A. and Thomas, D.J., 1996. Intraoceanic tectonics and the development of continental crust: 1.92–1.84 Ga evolution of the Flin Flon Belt, Canada; Geological Society of America Bulletin, v. 108, no. 5, p. 602-629.

Malehmir, A. and Bellefleur, G., 2016. Pros and cons of 2D crooked seismic profiles for deep mineral exploration-a comparison with 3D surveys in geologically complex mining environment; In EAGE/DGG Workshop on Deep Mineral Exploration, v. 2016, no. 1, p. 1-5.

Pandit, B. I., Hajnal, Z., Stauffer, M. R., Lewry, J., and Ashton, K. E., 1998. New seismic images of the crust in the central Trans-Hudson Orogen of Saskatchewan; Tectonophysics, v. 290, no. 3-4, p. 211–219, https://doi.org/10.1016/S0040-1951(98)00009-2

Schetselaar, E., Bellefleur, G., White, D., Bosman, S., Maxeiner, R., Reid, K. 2022a. Interpretation of the Denare Beach seismic profile, Saskatchewan: new insights into the 3D structural architecture of the Flin Flon – Glennie complex, 2022 Saskatchewan Open House, abstract.

Schetselaar, E.M., White, D., Boulanger, O., Craven, J.A., Bellefleur, G., and Ansari, S.M., 2022b. 3D regional-scale modelling of the Flin Flon – Glennie complex: preparatory data analysis and preliminary results, Manitoba and Saskatchewan; Geological Survey of Canada, Open File 8905, 33 p. https://doi.org/10.4095/330304

Storn, R. and Price, K., 1997. Differential evolution - a simple and efficient heuristic for global optimization over continuous spaces; Journal of global optimization, v. 11, no. 4, p. 341–359, https://doi.org/10.1023/A:1008202821328

Syme, E.C. and Bailes, A.H., 1993. Stratigraphic and tectonic setting of early Proterozoic volcanogenic massive sulfide deposits, Flin Flon, Manitoba; Economic Geology, v. 88, no. 3, p. 566-589.

Wu, J., 1996. Potential pitfalls of crooked-line seismic reflection surveys. Geophysics, v. 61, no. 1, p. 277-281.
Xie, Y., Gajewski, D., 2018. 3D wavefront attribute determination and conflicting dip processing; Geophysics, v. 83, no. 6, p. V325–V343, https://doi.org/10.1190/geo2017-0792.1

Yilmaz, O., 2001. Seismic data analysis: Processing, inversion, and interpretation of seismic data; Society of exploration geophysicists, https://doi.org/10.1190/1.9781560801580